Seventh International Conference on CFD in the Minerals and Process Industries
CSIRO, Melbourne, Australia
9-11 December 2009

THE ROLE OF PARTICLE SHAPE IN PNEUMATIC CONVEYING

James E. HILTON[1*], Paul W. CLEARY

[1] CSIRO Mathematical and Information Sciences, Clayton, Victoria 3169, AUSTRALIA
*Corresponding author, E-mail address: James.Hilton@csiro.au

ABSTRACT

Pneumatic conveying, in which granular materials are transported using a gas phase, is an important industrial process for bulk particulate transport. This is usually carried out in either a dilute phase, in which the particles are effectively suspended in the gas phase, or a dense phase, in which the particles move in a bulk flow. Dense phase conveying is becoming increasingly popular as it reduces collisional and abrasional forces on both the particles and the walls, reducing breakage and wear in the system. The motion of the particles is difficult to capture experimentally making computational simulation of such systems invaluable for understanding their dynamics.

Previous experimental and computational studies have investigated both horizontal and vertical dense conveying and the effect of gas flow velocity and pressure on the bulk particle flow rate. It has also been found that the formation and movement of slugs of particles in a wave-like motion in the direction of the flow accounts for the majority of the bulk flow in the system. However, most simulations have modelled the particles as spheres, which is a considerable approximation as many particles in industrial applications are non-spherical. We explore the role of shape in horizontal dense phase pneumatic conveying by investigating how cubical and elliptical particles change the dynamics of the system. We compare both slug formation and the movement of slugs to the spherical case and show the bulk flow is highly sensitive to particle shape.

NOMENCLATURE

$A_\perp$	particle flow projected area
c_{ls}	shear lift coefficient
c_{lm}	rotational lift coefficient
c_d	drag coefficient
C	particle damping coefficient
D	duct equivalent diameter
$\mathbf{D}$	rate of deformation tensor
$\mathbf{F}_{ci}$	particle collisional force
$\mathbf{F}$	particle force
k	particle spring stiffness
m	particle mass
p	pressure
q	super-quadric exponent
r	characteristic particle radius
Re	particle Reynolds number
$\mathbf{T}$	particle torque
$\mathbf{u}$	gas velocity
$\mathbf{u}_r$	relative particle velocity
$\mathbf{v}$	particle velocity
$\delta\mathbf{x}$	particle overlap
ε	voidage fraction
ρ	gas density
ρ_p	particle density
ρ_b	bulk particle density = $(1-\varepsilon)\rho_p$
μ	particle friction coefficient
η	gas viscosity
χ	drag correction coefficient
Φ	particle sphericity
$\Phi_\perp$	particle crosswise sphericity
$\boldsymbol{\omega}_f$	fluid vorticity
$\boldsymbol{\omega}_p$	particle spin
$\boldsymbol{\omega}_r$	relative particle spin

INTRODUCTION

The rapid transportation of large volumes of granular matter is a prime concern in industry. A popular method is the use of pneumatic conveying, in which the granular matter is driven along pipes using air flow. The bulk grain motion in pneumatic conveying can occur in several regimes depending on parameters such as grain inflow rate, imposed gas flow rate, grain density and diameter (Molerus, 1996). The motion is usually classified into two phases; dilute phase, where the grains move as a suspension in the conveying gas, and dense phase, where the grains are subject to long lasting collisions and move in bulk along the pipe (Jones and Williams, 2008).

Large particles with high density, categorised as type D in the Geldart scheme (Geldart, 1973), typically move as a sequence of solid plugs within the pipe. This is known as slug flow and is a dense phase flow mode. In this mode particles initially sediment in a layer over the bottom of the pipe. The particle bed then rises to fill the bore of the pipe and the pressure builds up behind this blockage, pushing a slug out from the front of the particle bed. If the pipe in front of the slug is empty then the slug collapses into a layer of particles and the sequence repeats. A steady sequence of slugs only occurs if particles have already been deposited over the length of the pipe (Tomita et al., 1981). Due to low power consumption and particle attrition (Pan and Wypych, 1997), this plug flow mode has received a large amount of attention computationally and experimentally. Experimentally, plug flow regimes can be determined from visual inspection of the flow using a transparent tube for the granular transport (Wen and Simons, 1959, Woods et al., 2008, Tomita et al., 2008). The presence of slugs can also be inferred using pressure measurements (Li et al., 2002) from a series of pressure transducers attached along the transporting pipe. Plugs have also been experimentally measured using capacitance computed tomography in which radial electrodes measure the electric field around a pipe during conveying. By measuring the capacitance between each electrode the permittivity, and hence particle concentration, can be computationally determined (Takei et al., 2004).

Plug flow formation and collapse was first computationally modelled by Tsuji et al. (1992), who found good agreement with the predicted and measured stationary layer as well as overall plug dynamics. Fraige and Langston (2006) modelled pneumatic conveying and reported good comparison to experimental observations. However, their model used a steady state assumption for the gas flow field, and based the pressure drop on the Ergun relation rather than any computed flow field. Tsuji (2007) later extended his original work to a multiscale approach and demonstrated applicability in a number of areas including plug flow in pneumatic conveying. Strauß et al., (2007) compared horizontal plug formation to vertical plug formation, and investigated shear layering within the plug as well as plug collapse. Kuang et. al, (2008) carried out detailed measurements of pressure drops as well as internal force networks within slugs. They showed that the slug is governed by axial particle fluid force, and proposed an empirical relation between porosity and particle flow rate over different gas flow rates. Sakai et al. (2009) have recently demonstrated plug flow in a multiscale discrete element model.

As their size and density are decreased, particles fall into the Geldart type B category. In pneumatic conveying particles of this type become suspended within the gas and particle transport is almost entirely due to aerodynamic drag. This mode is the dilute phase transport regime, with losses mainly occurring from inter-particle and particle-wall collisions. This dilute phase can cause high material degradation in both particles and pipeline due to these collisions and is typically avoided in industrial systems for the transport of fragile materials. The mechanics of this regime are well understood and formed the basis for the earliest pneumatic conveying models.

As particle size is decreased further still, to Geldart type A and C, the particles move as a series of rolling dunes. This mode is also a dense phase flow mode but the mechanics of conveying are very different to the plug flow regime. This mode was first described by Wen and Simons (1959) and later investigated by Laouar and Molodtsof (1998). In contrast to the plug flow regime this rolling dune regime has received little attention.

The effect of shape on pneumatic conveying has not been investigated. A related problem of ellipsoidal particles in channel flow has been considered by Mortensen et al. (2008), although not in the context of pneumatic conveying. We investigate the dynamics of the conveying as well as the transition between the various pneumatic conveying regimes for steady-state conveying using different shaped particles. We show that the transitions are highly sensitive to particle shape due to the change in bulk packing fraction as the shape is varied.

COMPUTATIONAL MODEL

Our computational model uses a Lagrangian particle scheme, called the Discrete Element Method (DEM), first formulated by Cundall and Strack (1979). This is coupled to an Eulerian scheme for fluid flow through packed particle beds. The first coupled DEM and fluid method was carried out by Tsuji (1993), who investigated a two-dimensional gas-solid fluidised bed of spherical particles. Two types of DEM-gas models have been proposed, the pressure gradient force (PGF) and fluid density-based buoyancy models. Kafui (2002) has shown that the PGF model gives the best agreement with empirical pressure drop and gas velocity data, and this method is used in our simulations.

Lift Forces

For small particles, lift forces are crucial to the dynamics of the system. We incorporate both shear (Saffman) lift and rotational (Magnus) lift forces into our model. The shear lift force, $\mathbf{F}_{LS}$, on an isolated spherical particle subject to a relative fluid velocity $\mathbf{u}_r$ is given by a generalisation of Saffman's 1D form (1964) by Drew (1976):

$$\mathbf{F}_{LS} = 6.46 c_{ls} r^2 \sqrt{\rho\mu}\, \frac{\mathbf{u}_r \cdot \mathbf{D}}{\sqrt{\mathbf{D}}} \tag{1}$$

where the rate of deformation tensor is $\mathbf{D} = (\nabla\mathbf{u}_r + \nabla\mathbf{u}_r^{\mathrm{T}})$. We use an empirical correction to the lift coefficient given by Mei (1992):

$$c_{ls} = \begin{cases} e^{-\mathrm{Re}/10} - 0.3314\sqrt{\alpha}\left(e^{-\mathrm{Re}/10}+1\right) & \mathrm{Re} \le 40 \\ 0.0524\sqrt{\alpha\,\mathrm{Re}} & \mathrm{Re} > 40 \end{cases} \tag{2}$$

where the particle Reynolds number is $Re = 2r\rho|\mathbf{u}_r|/\mu$ and the coefficient $\alpha = |\mathbf{D}|r/|\mathbf{u}_r|$. An isolated spherical particle subject to a relative spin $\boldsymbol{\omega}_r = \frac{1}{2}\boldsymbol{\omega}_f - \boldsymbol{\omega}_p$ is also subject to a Magnus lift force, $\mathbf{F}_{LM}$, given by:

$$\mathbf{F}_{LM} = \tfrac{1}{2} c_{lm} \pi r^2 \rho \frac{\boldsymbol{\omega}_r \times \mathbf{u}_r}{|\boldsymbol{\omega}_r|} \tag{3}$$

with an empirical correction given by Lun and Lui (1997):

$$c_{lm} = \begin{cases} 2r|\boldsymbol{\omega}_r| & \mathrm{Re} \le 1 \\ 2r|\boldsymbol{\omega}_r|\left(0.178 + 0.822\,\mathrm{Re}^{-0.522}\right) & \mathrm{Re} > 1 \end{cases} \tag{4}$$

Drag Forces

The drag force exerted on a particle in a multi-particle system with corrections due to Di Felice (1994) is:

$$\mathbf{F}_D = \tfrac{1}{2} c_d \rho |\mathbf{u}_r|^2 \varepsilon^{-\chi} A_\perp \mathbf{u}_r \tag{5}$$

where χ is given by:

$$\chi = 3.7 - 0.65 \exp\left\{-\tfrac{1}{2}\left(1.5 - \log \mathrm{Re}\right)^2\right\} \tag{6}$$

Holzer *et al.* (2008) give the following drag coefficient for single non-spherical particles, based on correlations to experimental data:

$$c_d = \frac{8}{\mathrm{Re}}\left(\frac{1}{\sqrt{\Phi_\perp}} + \frac{2}{\sqrt{\Phi}}\right) + \frac{3}{\mathrm{Re}\sqrt{\Phi^{\frac{3}{4}}}} + \frac{1}{\Phi_\perp} 0.42 \times 10^{0.4(-\log\Phi)^{0.2}} \tag{7}$$

where the regular sphericity, Φ, is the ratio between the surface area of the volume equivalent sphere and the surface area of the considered particle and the crosswise sphericity, $\Phi_\perp$, is the ratio between the cross-sectional area of the volume equivalent sphere, A, and the projected cross-sectional area of the considered particle perpendicular to the flow, $A_\perp$ giving $\Phi_\perp = A / A_\perp$. This is an approximation to their more accurate expression where crosswise sphericity has replaced lengthwise sphericity. Eq. (7) is valid over the full practical range of Re.

Particles are also subject to Stokesian rotational drag, given by:

$$\mathbf{T}_D = 8\pi\eta r^3 \boldsymbol{\omega}_r \tag{8}$$

Particle Motion Equations

The DEM for particles has been applied to simulate a wide range of industrial processes (see Cleary, 2004 for examples). The particle-particle contact force, $\mathbf{F}_{ci}$, is determined by particle overlap information in the discrete element simulation using a soft-sphere linear spring, dashpot and slider approximation. This force is the sum of a normal force $\mathbf{F}_n$ and a tangential force $\mathbf{F}_t$. The normal force is determined from the particle overlap $\delta\mathbf{x}$ and relative normal velocity $\mathbf{v}_n$:

$$\mathbf{F}_n = -k_n\delta\mathbf{x} + C_n\mathbf{v}_n \tag{9}$$

The tangential force is determined from the Coulomb friction limit and relative tangential velocity $\mathbf{v}_t$:

$$\mathbf{F}_t = \min\left\{\mu\mathbf{F}_n, k_t\int \mathbf{v}_t dt + C_t\mathbf{v}_t\right\} \tag{10}$$

The linear and angular accelerations are numerically integrated for each particle *i*. These are given by:

$$m_i\frac{d\mathbf{v}_i}{dt} = \mathbf{F}_{ci} + \mathbf{F}_{LS} + \mathbf{F}_{LM} + \mathbf{F}_D + \mathbf{F}_P + m_i\mathbf{g} \tag{11}$$

$$I_i\frac{d\boldsymbol{\omega}_i}{dt} = \mathbf{T}_{ci} + \mathbf{T}_D \tag{12}$$

The forces consist of a solid particle-particle contact force, $\mathbf{F}_{ci}$, as well as the fluid-particle interaction forces, the gradient of the fluid pressure, $\mathbf{F}_P$, and the gravitational force. The torque consists of the drag torque plus the particle-particle coupling torque, $\mathbf{T}_{ci}$.

Fluid Equations

We use constitutive equations for gas flow through a porous bed for modelling the system, where the porosity is explicitly calculated from the DEM simulation at each timestep. The choice of fluid-particle drag relations used to link the particle model with the gas phase is of great importance to the accuracy of the simulation. There currently is no consensus on the most accurate form of the drag force at a given Reynolds number and packing fraction (Beetstra et al., 2007), but the relations of Ergun (1952) or Wen and Yu (1966) are most often used.

The constitutive equations for the PGF gas flow model through a porous bed were derived by Anderson and Jackson (1967), and are given by Kafui as:

$$\frac{\partial(\varepsilon\rho)}{\partial t} + \nabla\cdot(\varepsilon\rho\mathbf{u}) = 0 \tag{13}$$

$$\frac{\partial(\varepsilon\rho\mathbf{u})}{\partial t} + \nabla\cdot(\varepsilon\rho\mathbf{u}\mathbf{u}) = -\varepsilon\nabla p - \mathbf{f}_{fp} - \nabla\cdot(\varepsilon\boldsymbol{\tau}) + \varepsilon\rho\mathbf{g} \tag{14}$$

These can be re-formulated for the superficial gas velocity $\mathbf{u}' = \varepsilon\mathbf{u}$ by assuming the gas density is constant to give:

$$\frac{\partial\varepsilon}{\partial t} = -\nabla\cdot\mathbf{u}' \tag{15}$$

and expression (14) becomes:

$$\frac{\partial\mathbf{u}'}{\partial t} + \frac{1}{\varepsilon}(\mathbf{u}'\cdot\nabla)\mathbf{u}' + \mathbf{u}'\nabla\cdot\frac{\mathbf{u}'}{\varepsilon} = -\frac{1}{\rho}\left[\varepsilon\nabla p + \mathbf{f}_{fp} + \nabla\cdot(\varepsilon\boldsymbol{\tau})\right] + \varepsilon\mathbf{g} \tag{16}$$

The stress tensor is given by:

$$\boldsymbol{\tau} = -\eta\left[\left(\nabla\frac{\mathbf{u}'}{\varepsilon} + \nabla\frac{\mathbf{u}'^T}{\varepsilon}\right) - \frac{2}{3}\left(\nabla\cdot\frac{\mathbf{u}'}{\varepsilon}\right)\mathbf{I}\right] \tag{17}$$

where $\mathbf{I}$ is the identity tensor. These equations are discretised on a Cartesian grid over the simulation domain.

The procedure for the numerical calculation is firstly to determine the porosity at the new time step by calculating the volume distribution from the DEM particles. The velocity field is then calculated using Eq. (15), which gives the rate of change of porosity as divergence of the velocity, and Eq. (16) which gives the velocity field at the next timestep. Eq. (16) is solved using a variation of the pressure correction method.

PNEUMATIC CONVEYING

We consider particle sizes of 400 μm equivalent spherical radius and density 2700 kg/m^3, which spans Geldart groups B to D. Our setup is a square duct of length 10 cm with width and height of 1 cm, (see Fig. 1).

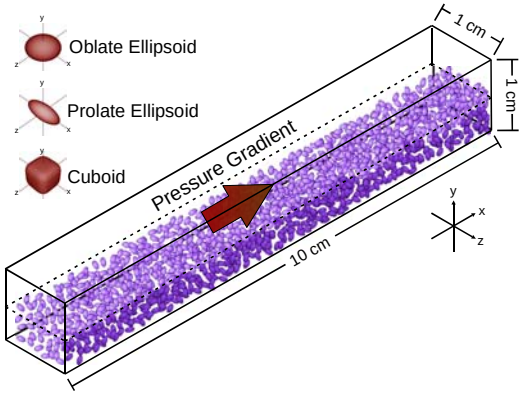

Figure 1: Schematic diagram of experimental set-up. Inset shows particle types considered in the simulations.

The lower half of the duct is evenly filled with particles of various shapes. For expressing various shapes, we use a super-quadric formulation, allowing us to simulate spherical to cuboidal particles by varying both a shape parameter and an aspect ratio. For our simulations we use a range of ellipsoids from oblate through spherical to prolate, as well as cuboidal particles.

The boundary conditions are periodic in the *x* and *z* directions for both the gas flow and the particles. The particles are subject to a solid boundary in the upper and lower *y* directions, and the fluid is subject to a zero velocity boundary condition. To drive the system a pressure gradient is imposed on the gas. The system pressure is split into a fluctuating and steady part, $p = p_f + p_s$, such that the gradient of p_s gives a driving pressure gradient. From Eq. (16) this gives:

$$\frac{\partial\mathbf{u}'}{\partial t} + \frac{1}{\varepsilon}(\mathbf{u}'\cdot\nabla)\mathbf{u}' + \mathbf{u}'\nabla\cdot\frac{\mathbf{u}'}{\varepsilon} = -\frac{1}{\rho}\left[\varepsilon\nabla p_f + \mathbf{f}_{fp} + \nabla\cdot(\varepsilon\boldsymbol{\tau})\right] + \varepsilon\left(\mathbf{g} - \frac{\nabla p_s}{\rho}\right) \tag{18}$$

The pressure gradient can therefore simply be imposed as a body force, along with gravity. The pressure gradient can be easily controlled in this way, and is transparent to periodic boundary conditions.

The equation for a super-quadric surface is:

$$r(\theta,\phi) = \begin{bmatrix} a\sin^q\theta\cos^q\phi \\ b\sin^q\theta\sin^q\phi \\ c\cos^q\theta \end{bmatrix} \tag{19}$$

where θ and ϕ are the zenith and azimuthal, respectively, in the shape frame and the shape parameter q controls the cubicity of the shape. Spheres have $q = 1$, and $q < 1$ gives shapes of increasing blockiness. The variables a, b and c are the aspect ratios along the x, y and z axes respectively.

Shape	q	a	b	c	Φ
Cuboid	0.5	1	1	1	0.956
Sphere	1	1	1	1	1
Prolate Ellipsoid	1	1	0.5	0.5	0.929
Prolate Ellipsoid	1	1	0.7	0.7	0.979
Prolate Ellipsoid	1	1	0.9	0.9	0.998
Oblate Ellipsoid	1	1	0.9	1	0.998
Oblate Ellipsoid	1	1	0.7	1	0.977
Oblate Ellipsoid	1	1	0.5	1	0.913

Table 1: Parameters for shapes investigated.

We use a shape parameter of $q = 0.5$ for our cuboidal particles, which is the lowest shape in the upper inset of Fig 1. The shape parameters are summarised in Table 1. All ellipsoidal particles used had the equivalent volume of a 400 μm radius sphere, and the cuboidal particles had the equivalent volume of a 300 μm radius sphere.

The pressure gradients chosen, $|\nabla p_s/\rho|$ ranged from 0.25 km/s^2 to 7.5 km/s^2 in increasing increments to capture the behaviour of the bed over a range of pressure gradients. This range is chosen to match pressure drops up to values measured by Laouar et al. (1998), (which were around 10 kPa/m in their experiments).

PARTICLE DYNAMICS

Spherical particles

The behaviour of the system was first investigated for spherical particles. A series of experiments at fixed pressure gradients were carried out, where the simulations were run until steady state flow was attained.

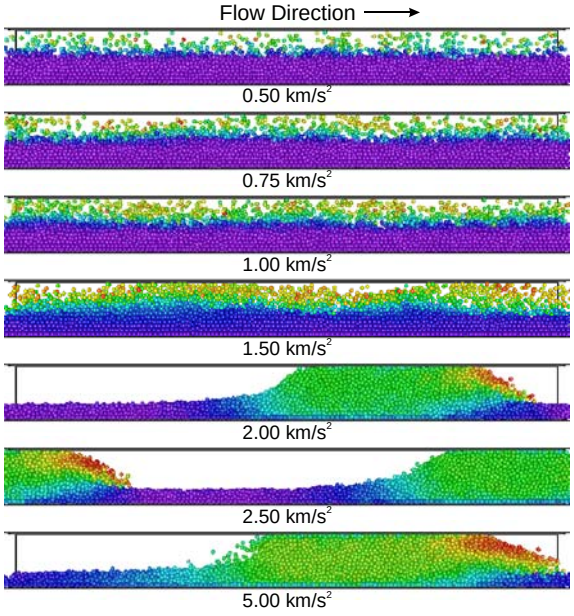

Figure 2: Flow modes 0.5 s from start-up for spherical particles for $|\nabla p_s/\rho|$ from 0.5 km/s^2 to 50 km/s^2, coloured by velocity magnitude (with red as high speed, green as intermediate and purple stationary). The images are taken across the periodic slice.

The bed is stationary for pressure gradients giving a gas flow under the particle saltation velocity, which is around 0.25 m/s using Dallavalle's (1942) expression. For gas flow velocities above the saltation velocity the particles lift off from the bed and are carried along by the gas. At low pressure gradients the bed is stationary and the steady state flow is a suspended layer of saltating particles moving over this fixed bed. This is shown in the top frame of Fig. 2 for a gradient of 0.50 km/s^2.

At higher pressure gradients the upper layer of the fixed bed begins to shear and the steady state flow is a sequence of small rolling dunes underneath a layer of saltating particles. Large scale waves also begin to appear as the pressure gradient is raised. These effects can both be seen for the 0.75 km/s^2 and 1.00 km/s^2 simulations in Fig. 2. These large scale waves grow as the pressure gradient is increased, as seen in the 1.50 km/s^2 simulation. The shear layer also extends to the bottom of the bed resulting in net bed motion. The growth of these waves then triggers a transition into steady state slug flow, as shown for the 2.00 km/s^2, 2.50 km/s^2 and 5.00 km/s^2 cases. Three flow modes can be identified. These are a thin (or non-existent) shear layer over a stationary bed, which we label mode A, a full shear layer across the bed resulting in a moving bed, which we label mode B, and slug flow, which we label mode C.

Non-spherical particles

The behaviour of the system was also investigated for non-spherical particles by carrying out the same sequence of experiments at fixed pressure gradients until steady state flow was reached.

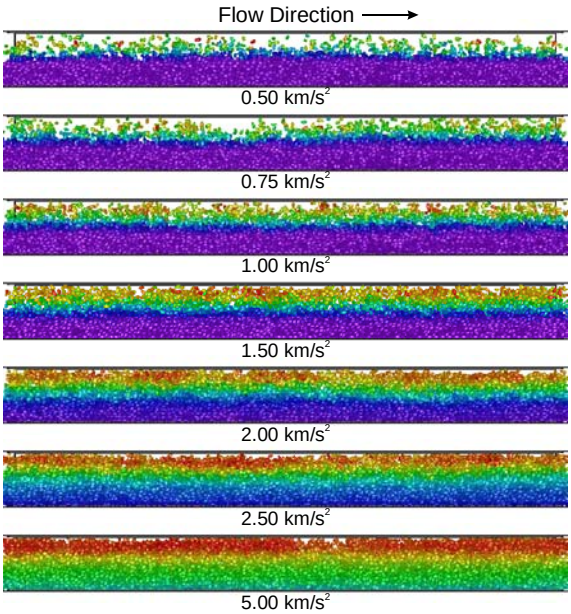

Figure 3: Flow modes 0.5 s from start-up for prolate ellipsoidal particles with $b = c = 0.5$ for $|\nabla p_s/\rho|$ from 0.25 km/s^2 to 50 km/s^2, coloured by velocity magnitude.

A small change in the shape of the particle was found to prevent slug flow from occurring. A transition to slug flow was only observed for oblate ellipsoids with $b = 0.9$. A further flow mode, which we label D, was also observed. In this mode the upper suspended upper layer appeared to grow to fill the system, resulting in sheared

dilute dune flow filling the entire domain. This is shown at 2.5 and 5.0 km/s^2 in Fig. 3.

The flow behaviour for the ellipsoidal particles is summarised in the phase diagram shown in Fig. 4. The slug flow regime exists as an island between the moving bed regime (B) and the dilute dune flow regime (D), with high and low aspect ratio ellipsoids transitioning directly between these regimes. Cuboidal particles show very similar behaviour to high aspect ratio ellipsoidal particles, transitioning directly from moving bed flow directly to dilute dune flow. The shear layer, however, is much thinner for cuboidal particles at the same pressure gradient.

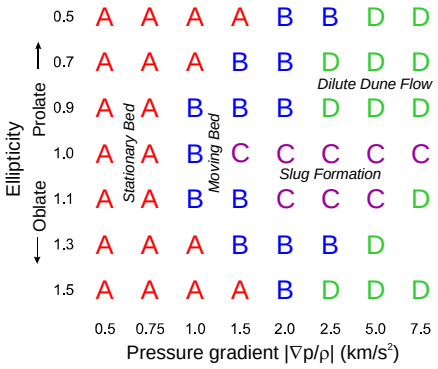

Figure 4: Flow modes 0.5 s from start-up for prolate ellipsoidal particles with $b = c = 0.5$ for $|\nabla p_s/\rho|$ from 0.25 km/s^2 to 50 km/s^2.

Fig 5 shows a cross-section of the bed for spherical, prolate ellipsoidal, cuboidal and oblate ellipsoidal particles 0.3 s after start-up for a pressure gradient of 2.5 km/s^2. The spherical particles have formed a slug, but the oblate ellipsoids and the cuboidal cases both have particles in a thin dilute dune phase over a deep fixed bed. The prolate ellipsoids can be seen to be in the moving bed regime, with a non-stationary lower layer.

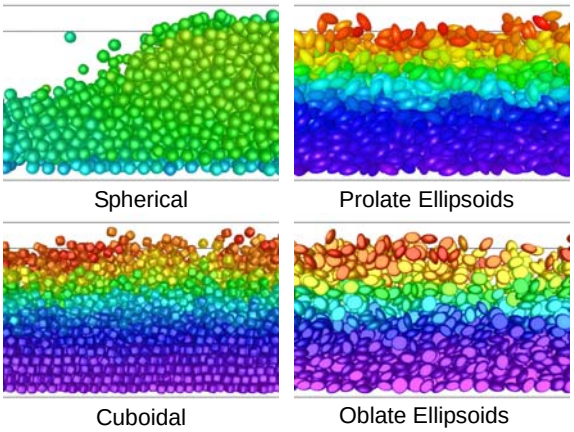

Figure 5: Bed cross section for shaped particles at a pressure gradient of pressure gradient of 2.5 km/s^2, 0.3 s after start-up, coloured by relative velocity magnitude.

EFFECT OF SHAPE

The transition to slug flow can clearly be seen as a discontinuity in the average gas velocity over the bed, as shown for particles of varying ellipticity in Fig.6.

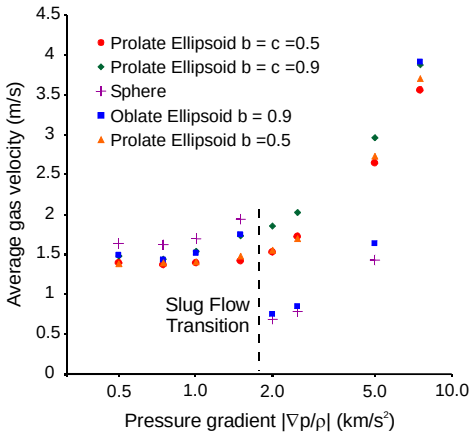

Figure 6: Average gas velocity against logarithmic pressure gradient $|\nabla p_s/\rho|$ from 0.5 km/s^2 to 75 km/s^2; for ellipsoidal particles of varying aspect ratio.

During slug flow the overall velocity is lower but the form of the curve is similar to the non-slugging cases. Since the curve in the slugging phase is entirely dominated by the percolation of gas through the bed, this suggests that the curve in the non-slugging phase is governed by the percolation through the bed plus a constant gas flow over the top of the bed. The gas fluidisation velocity over the bed is given by the Ergun equation:

$$\frac{dp}{dy} = \left(\frac{75\eta}{r}(1-\varepsilon) + 1.75\rho v_f\right)\frac{(1-\varepsilon)}{\varepsilon^3}\frac{v_f}{2r} \qquad (20)$$

Dixon (1979) proposed that slugs will only form and be stable if this fluidisation velocity is less than the slug or dune velocity. The slug velocity can be determined from a expression given by Yang (1976):

$$v_{slug} = 0.35(K g D)^{0.5} \qquad (21)$$

where the constant K is 1 for slug velocity and 2 for dune velocity. As we are considering the transition from dunes to slugs we take the velocity to be the dune velocity. The fluidisation velocity is given by the Ergun equation with pressure gradient $\rho_b \times g$:

$$\rho_b = \left(\frac{75\eta}{r}(1-\varepsilon) + 1.75\rho v_f\right)\frac{(1-\varepsilon)}{\varepsilon^3}\frac{v_f}{2gr} \qquad (22)$$

The critical curve for stable slug flow can be determined by substitution of Eq. (21) into Eq. (22), giving:

$$\rho_b = 4.19\frac{\eta\sqrt{2D}}{r^2}\frac{(1-\varepsilon)^2}{\varepsilon^3} + 0.2144\frac{\rho D}{r}\frac{(1-\varepsilon)}{\varepsilon^3} \qquad (23)$$

Shape	a	b	c	ε	ρ_b
Prolate Ellipsoid	1	0.5	0.5	0.3693	1702.81
Prolate Ellipsoid	1	0.7	0.7	0.3697	1701.90
Prolate Ellipsoid	1	0.9	0.9	0.3993	1621.86
Sphere	1	1	1	0.4161	1576.44
Oblate Ellipsoid	1	0.9	1	0.4012	1616.50
Oblate Ellipsoid	1	0.7	1	0.3772	1681.67
Oblate Ellipsoid	1	0.5	1	0.3767	1682.99

Table 2: Porosity and bulk density for ellipsoids.

Eq. (23) is plotted in Fig. 7 for porosities calculated from the packed ellipsoidal beds in the initial state, given in Table 2. Only ellipsoidal particles with ellipticity between 0.9 and 1.1 lie above the critical curve, meaning

that slugs are only predicted to form for ellipsoids with ellipticity in this range. This agrees well with the results of our simulations, as we found slugs formed for ellipticity of 1.0 to 1.1. We did not, however, find slug formation for particles with ellipticity 0.9 although the theory predicts that slugs should form at this value.

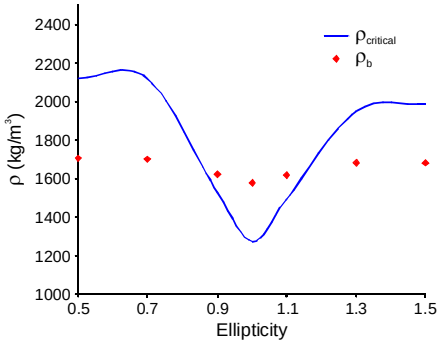

Figure 7: Critical bulk density curve from Dixon's argument plotted against values for ellipsoidal particles.

CONCLUSION

Our simulations have shown that altering the shape of a particle by a small amount can significantly affect the bulk dynamics of a pneumatic conveying system. The change in shape of a particle causes the packing fraction to change, altering the bulk density of the particle bed. This, in turn, alters the fluidisation velocity and can cause slugs to become unstable. This has been confirmed using Dixon's method, which has not previously been used for shaped particles. Simply applying expressions derived from empirical relations for spherical particles may not give a correct prediction of a pneumatic flow mode. Particle shape should therefore be taken into account in the consideration and design of these systems.

REFERENCES

ANDERSON, T.B. and JACKSON, R., (1967), "A fluid mechanical description of fluidised beds", *Industrial and Engineering Chemistry Fundamentals*, **6**, p527

BEETSTRA, R., VAN der HOEF M.A. and KUIPERS, J.A.M., (2007), "Drag force of intermediate Reynolds number flow past mono- and bidisperse arrays of spheres". *A. I. Ch. E.*, **53**, p489

CLEARY, P.W., (2004), "Large scale industrial DEM modelling", *Engineering Computations*, **21**, p169

CUNDALL, P. A. and STRACK, O. D. L., (1979), "A discrete numerical model for granular assemblies", *Geotechnique*, **29**, p47

DALLAVALLE, J. M. (1942), "The theory and practice of pneumatic conveying", *Heat and Ventil.*, **39**, p28

Di FELICE, R., (1994) "The voidage function for fluid-particle interaction systems", *Int. J. Multiphase Flow*, **20**, p153

DIXON, G., (1979), "The impact of powder properties on dense phase flow", *Proceedings of the International Conference on Pneumatic Conveying*

DREW. D., (1976), "Two-phase flows: Constitutive equations for lift and brownian motion and some basic flows", *Archive for Rational Mechanics and Analysis*, **62**, p149

ERGUN, S., (1952), "Fluid flow through packed columns", *Chem. Eng. Prog.*, **48**, p89

FRAIGE, F. Y. and LANGSTON, P. A., (2006), "Horizontal pneumatic conveying: A 3d distinct element model", *Granular Matter*, **8**, p67

GELDART, D., (1973), "Types of gas fluidisation", *Powder Technology*, **7**, p285

HÖLZER, A. and SOMMERFELD, M., (2008), "New simple correlation formula for the drag coefficient of non-spherical particles", *Powder Technology*, **184**, p361

JONES, M. G. and WILLIAMS, K. C., (2008), "Predicting the mode of flow in pneumatic conveying systems – a review", *Particuology*, **6**, p289

KAFUI, D. K., THORNTON and C. ADAMS, M. J., (2002), "Discrete particle-continuum fluid modelling of gas-solid fluidised beds", *Chem. Eng. Sci.*, **57**, p2395

KUANG, S. B., CHU, K. W., YU, A. B., ZOU, Z. S. and FENG, Y. Q., (2008), "Computational investigation of horizontal slug flow in pneumatic conveying", *Ind Eng. Chem. Res.*, **47**, p470

LAOUAR, S. and MOLODTSOF, Y., (1998), "Experimental characterization of the pressure drop in dense phase pneumatic transport at very low velocity", *Powder Technology*, **95**, p165

LI, J., PANDIELLA, S. S., WEBB C., McGLINCHEY, D., COWELL, A., XIANG, J., KNIGHT, L. and PUGH, J., (2002), "An experimental technique for the analysis of slug flows in pneumatic pipelines using pressure measurements", *Particulate Sci. Tech.*, **20**, p283

LUN, C. K. K. and LIU, H. S., (1997), "Numerical simulations of dilute turbulent gas-solid flows in horizontal channels", *Int. J. Multiphase Flow*, **23**, p575

MEI, R., (1992), "An approximate expression for the shear lift for on a spherical particle at finite Reynolds number", *Int. J. Multiphase Flow*, **18**, p145

MOLERUS, O., (1996) "Overview: Pneumatic transport of solids", *Powder Technology*, **88**, p309

MORTENSEN, P., ANDERSSON, H. I., GILLISSEN, J. J. J. and BOERSMA, B. J. (2008), "Dynamics of prolate ellipsoidal particles in a turbulent channel flow", *Phys. Fluids*, **20**, 093302

PAN, R. and WYPYCH, P. W., (1997), "Pressure drop and slug velocity in low-velocity pneumatic conveying of bulk solids", *Powder Technology*, **94**, p123

SAFFMAN, P. G., (1964), "The lift on a small sphere in a slow shear flow", *J. Fluid Mech*, **22**, p385

SAKAI, M. and KOSHIZUKA, S., (2009) "Large-scale discrete element modeling in pneumatic conveying", *Chem. Eng. Sci.*, **64**, p533

STRAUß, M., McNAMARA, S. and HERRMANN, H. J., (2007), "Plug conveying in a horizontal tube", *Granular Matter*, **9**, p35

TAKEI, M., OCHI, M. and SAITO, Y., (2004) "Image extraction of particle concentration at the plug front using 3D wavelets and comparison with LDV", *Powder Tech.*, **142**, p70

TOMITA, Y., JOTAKI, T. and HAYASHI, H., (1981), "Wavelike motion of particulate slugs in a horizontal pneumatic pipeline", *Int. J. Multiphase Flow*, **7**, p151

TOMITA, Y., AGARWAL, V. K., ASOU and H., FUNATSU, K., (2008), "Low velocity pneumatic conveying in horizontal pipe for coarse particles and fine powders", *Particuology*, **6**, p316

TSUJI, Y., T., TANAKA, T. and ISHIDA, T., (1992), "Lagrangian numerical simulation of plug flow of cohesionless particles in a horizontal pipe", *Powder Tech.*, **71**, p239

TSUJI, Y., KAWAGUCHI, T. and TANAKA, T., (1993), "Discrete particle simulation of two-dimensional fluidized bed", *Powder Technology*, **77**, p79

TSUJI, Y. (2007), "Multi-scale modeling of dense phase gas-particle flow", *Chem. Eng. Sci.*, **62**, p3410

WEN, C. and SIMONS, H. P., (1959), "Flow characteristics in horizontal fluidized solids transport", *A. I. Ch. E.*, **5**, p263

WEN, Y. C. and YU, Y. H., (1966), "Mechanics of Fluidization", *Chem. Eng. Progress Symposium Series*, **62**, p100

WOODS, J. A., THORPE, R. B. and JOHNSON, S. E., (2008), "Horizontal pneumatic conveying from a fluidized bed", *Chem. Eng.Sci.*, **63**, p1741

YANG, W. C. (1976), *Proceedings of BHRA Pneumotransport 3*, pE5